



# Isolated Zr Surface Sites on Silica Promote Hydrogenation of CO<sub>2</sub> to CH<sub>3</sub>OH in Supported Cu Catalysts

## Journal Article

### Author(s):

Lam, Erwin; [Larmier, Kim](#) ; Wolf, Patrick; Tada, Shohei; Safonova, Olga V.; [Copéret, Christophe](#) 

### Publication date:

2018-08-22

### Permanent link:

<https://doi.org/10.3929/ethz-b-000284067>

### Rights / license:

[In Copyright - Non-Commercial Use Permitted](#)

### Originally published in:

Journal of the American Chemical Society 140(33), <https://doi.org/10.1021/jacs.8b05595>

# Isolated Zr Surface Sites on Silica Promotes CO<sub>2</sub>-to-CH<sub>3</sub>OH Conversion in Supported Cu Catalysts

Erwin Lam†, Kim Larmier†, Patrick Wolf†, Shohei Tada†, Olga V. Safonova<sup>‡</sup>, Christophe Copéret<sup>\*,†</sup>

†Department of Chemistry and Applied Biosciences, ETH Zurich, Vladimir Prelog Weg 1-5, CH-8093 Zurich, Switzerland

<sup>‡</sup>Paul Scherrer Institute, CH-5232 Villigen, Switzerland

## 2.1 Introduction

The selective CO<sub>2</sub> hydrogenation to CH<sub>3</sub>OH has recently received an increasing attention as a way to mitigate the increase of atmospheric CO<sub>2</sub> by its incorporating in a carbon cycle within the concept of methanol economy.<sup>[1-5]</sup> Among various metals, copper-based catalysts display relatively good activity and selectivity for this reaction.<sup>[3, 6-13]</sup> In particular, copper promoted by zinc oxide/alumina (Cu/ZnO/Al<sub>2</sub>O<sub>3</sub>)<sup>[14-21]</sup> or supported on zirconia (Cu/ZrO<sub>2</sub>)<sup>[22-36]</sup> have shown promising activity and selectivity. The selectivity toward CH<sub>3</sub>OH has been ascribed to a synergistic effect between the promoter/support and copper. By comparison, copper supported on silica (Cu/SiO<sub>2</sub>), a rather inert support, shows significantly lower activity and selectivity towards CH<sub>3</sub>OH, favoring CO formation.<sup>[22-24, 32-33]</sup>

In the case of Cu/ZnO/Al<sub>2</sub>O<sub>3</sub>, the specific catalyst performance has been mostly attributed to the formation of a CuZn alloy, due to strong metal support interaction (SMSI).<sup>[37-43]</sup> In contrast, the origin of the high activity/selectivity for CH<sub>3</sub>OH with Cu/ZrO<sub>2</sub> is still under debate. It has been ascribed to the interface between copper and zirconia due to assisted hydrogenation of surface intermediates into CH<sub>3</sub>OH.<sup>[24]</sup> However, the nature of the Zr site participating in CH<sub>3</sub>OH formation, Zr(III) vs. Zr(IV),<sup>[24, 44]</sup> is still a matter of discussion. Oxygen vacancies that may form on ZrO<sub>2</sub><sup>[44-46]</sup> and the electronic charge transfer between copper particles and the support<sup>[47]</sup> have alternatively been proposed as key properties of the support, which could explain the improved performances. One critical issue in understanding the role of the ZrO<sub>2</sub> support at a molecular level is the difficulty to probe specifically the reactivity of zirconium surface sites in the presence of bulk and therefore to distinguish the local properties of zirconium atoms on the surface with collective properties of bulk oxide related to the band gap and its ability to give and loose electrons under reducing conditions.<sup>[48]</sup>



(Scheme 1 and Figure A.1a). The appearance of a vibration band at 3790  $\text{cm}^{-1}$  indicates the formation of Zr-OH groups.<sup>[58]</sup> Analysis of the supernatant after grafting shows that ca. 0.3 equiv.  $[\text{Zr}(\text{OSi}(\text{O}t\text{Bu})_3)_4]$  reacted with surface silanol groups (1.0 Si-OH/ $\text{nm}^2$ ) on  $\text{SiO}_2\text{-700}$  thus providing a material with 0.3 Zr/ $\text{nm}^2$ . In addition, the final thermal treatment also generates ca. 1.2 M-OH/ $\text{nm}^2$  (M=Si or Zr) according to titration with  $[\text{Mg}(\text{CH}_2\text{Ph})_2(\text{Et}_2\text{O})_2]$ .

$\text{Zr}_{0.9}@\text{SiO}_2$  readily reacts with  $[\text{Cu}(\text{OtBu})_4]$  via grafting on the surface hydroxyls, and the resulting material yields supported copper nanoparticles upon further treatment under  $\text{H}_2$  at 500 °C, Cu/ $\text{Zr}_{0.9}@\text{SiO}_2$  (Figure 2a). The corresponding supported copper nanoparticles are also prepared by the same approach (grafting followed by reduction under  $\text{H}_2$ ) on  $\text{SiO}_2\text{-500}$  and  $\text{ZrO}_2\text{-500}$  (partially dehydroxylated at 500 °C), respectively (Figure A.1b). Copper loadings are 4.19 wt% for  $\text{Zr}_{0.9}@\text{SiO}_2$  and  $\text{SiO}_2$ , and 2.33 wt% for  $\text{ZrO}_2$  as determined by ICP-OES. No crystalline  $\text{ZrO}_2$  or Cu phases are observed for  $\text{Zr}_{0.9}@\text{SiO}_2$  by powder-XRD (Figure A.2). For Cu/ $\text{ZrO}_2$ , the powder XRD pattern shows the presence of mainly tetragonal and minor monoclinic phases (Figure A.3). The specific surface area determined by  $\text{N}_2$  adsorption and BET analysis is 196 and 206  $\text{g m}^{-2}$  for Cu/ $\text{SiO}_2$  and Cu/ $\text{Zr}_{0.9}@\text{SiO}_2$ , respectively (Table 1), while it is 115  $\text{g m}^{-2}$  for Cu/ $\text{ZrO}_2$  (Table 1 entry 2). On Cu/ $\text{SiO}_2$  and Cu/ $\text{Zr}_{0.9}@\text{SiO}_2$  small and narrowly distributed nanoparticles with particles sizes of around 3 nm are observed by transmission electron microscopy (Figure 2b and Figure A.4). However, the poor contrast between Cu and  $\text{ZrO}_2$  prevented TEM analysis for Cu/ $\text{ZrO}_2$ . The amount of surface exposed copper atoms determined by  $\text{N}_2\text{O}$  titration are 50  $\mu\text{mol g}^{-1}$  for the silica based samples and 33  $\mu\text{mol g}^{-1}$  for Cu/ $\text{ZrO}_2$ . Overall, all the prepared silica-based samples show comparable physicochemical properties in terms of specific surface area, dispersion and particle size distribution.

To elucidate the nature of the zirconium sites, zirconium K-edge XAS are measured on the Cu/ $\text{Zr}_{0.9}@\text{SiO}_2$  and  $\text{Zr}_{0.9}@\text{SiO}_2$  samples. The zirconium K-edge X-ray absorption near edge structure (XANES) spectrum of  $\text{Zr}_{0.9}@\text{SiO}_2$  shows a pre-edge feature assigned to  $1s \rightarrow 4d$  transitions indicative of a non-centrosymmetric environment around zirconium.<sup>[59-62]</sup> Two inflexion points at the same positions as for the molecular precursor (18002.0 and 18013.2 eV) characteristic of Zr(IV) are observed (Table A.1).<sup>[59-60]</sup>

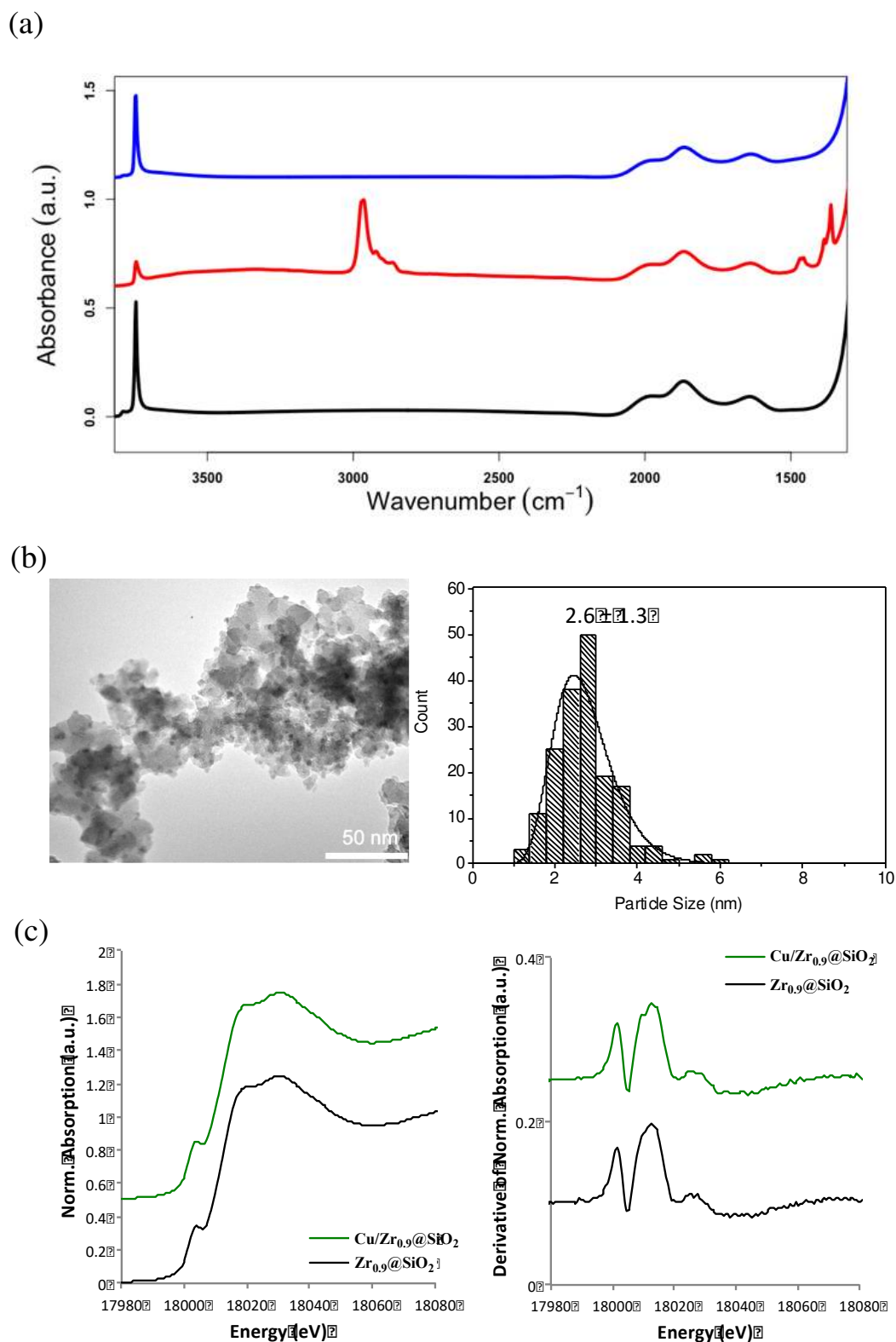


**Figure 2.** Characterization of  $\text{Cu/Zr}_{0.9}\text{@SiO}_2$  sample with (a) the IR spectrum of  $\text{Zr}_{0.9}\text{@SiO}_2$  before (black), after (red) grafting, and after reduction with  $\text{H}_2$  (blue), (b) particle size distribution and (c) Zr K-edge XANES spectra of  $\text{Zr}_{0.9}\text{@SiO}_2$  and  $\text{Cu/Zr}_{0.9}\text{@SiO}_2$ . left: normalized absorption, right: first derivative.

**Scheme 1.** Schematic procedure for grafting of  $[\text{Zr}(\text{OSi}(\text{OtBu})_3)_4]$  on  $\text{SiO}_2\text{-700}$  followed by thermal treatment at  $500\text{ }^\circ\text{C}$ , grafting and reduction of  $[\text{Cu}(\text{OtBu})_4]$ .

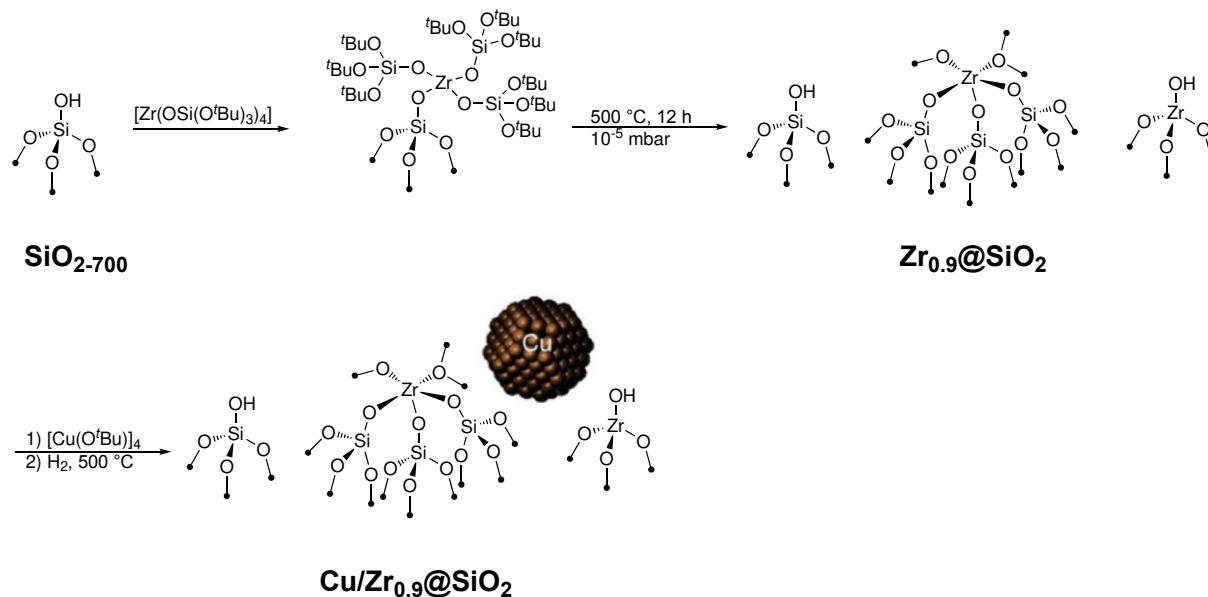


**Table 1.** Physicochemical properties of copper based catalysts.

Entry	Catalyst	Zr loading <sup>a)</sup> [wt%]	Cu loading <sup>a)</sup> [wt%]	Specific surface area <sup>b)</sup> [m <sup>2</sup> g <sup>-1</sup> ]	Surface copper <sup>c)</sup> [μmol g <sup>-1</sup> ]	Cu particle size distribution <sup>d)</sup> [nm]
1	Cu/SiO <sub>2</sub>	N/A	4.19	197	50/34	2.9 ± 1.3
2	Cu/ZrO <sub>2</sub>	N/A	2.33	115	33/17	N/A
3	Cu/Zr <sub>0.9</sub> @SiO <sub>2</sub>	0.96	4.19	206	50/50	2.6 ± 1.3

a) Determined by ICP-OES; b) determined from N<sub>2</sub> physisorption applying the BET theory; c) determined from N<sub>2</sub>O chemisorption on fresh/spent catalyst; d) determined by TEM of fresh catalyst.

After grafting of the copper complex and reduction under hydrogen at 500 °C, no change is observed in the zirconium K-edge XANES indicating that the treatment under H<sub>2</sub> at high temperature does not affect neither the oxidation state nor the local environment around the zirconium atoms (Figure 2c).

The shape of the edge is also clearly different from what is observed on bulk zirconia (Figure A.5), indicative of different environments of zirconium in the two samples. The particular shape of the XANES observed for Zr<sub>0.9</sub>@SiO<sub>2</sub> and Cu/Zr<sub>0.9</sub>@SiO<sub>2</sub> is assigned to isolated zirconium structures in a non-centrosymmetric environment, but dimeric zirconium species cannot be excluded.<sup>[59-60]</sup> The EXAFS spectra of Zr<sub>0.9</sub>@SiO<sub>2</sub> and Cu/Zr<sub>0.9</sub>@SiO<sub>2</sub> are identical and can be adequately fitted (Figure A.6) with a structure close to the one of its molecular precursor, with 5 oxygen neighbors on 2 different shells (around 1.95 and 2.3 Å) likely originating from the Zr-O-Si bridges inherited from the parent molecular precursor. The data is consistent with the proposed structure given in Scheme 1. Thus, a non-centrosymmetric environment with reduced number of oxygen neighbors is observed in line with the appearance of the pre-edge feature in the XANES spectrum. The feature around 3 Å required the addition of Zr-Si and Zr-O-Si scattering paths, similar to what is observed on the molecular precursor [Zr(OSi(O*t*Bu)<sub>3</sub>)<sub>4</sub>] (Figure A.6). Note that the spectrum could not be properly fitted by including Zr-Zr paths in addition or in substitution of the Zr-Si/Zr-O-Si paths. Thus, XANES and EXAFS confirm that zirconium has a structure inherited from the parent molecular complex and that it remains highly dispersed, predominantly isolated, at the surface of silica, even after the thermal treatment and the reduction step, both carried out at 500 °C.

Pyridine adsorption is also performed to assess the surface acidic properties of the support: after adsorption at room temperature and evacuation at 10<sup>-5</sup> mbar for 15 min at 150 °C, the solid-state <sup>15</sup>N NMR spectrum (Figure A.7) shows two signals at 244 and 276 ppm. The signal at 244 ppm is assigned to Lewis acidic sites and the signal at 276 ppm can be assigned to either weakly Lewis acidic sites or hydrogen bonded pyridine.<sup>[63]</sup> This further confirms the introduction of surface Zr (IV) Lewis acidic sites at the surface of silica.

## 2.2 Catalytic Performances

All Cu catalysts are then evaluated in CO<sub>2</sub> hydrogenation at 25 bar and 230 °C. The zirconium-containing samples exhibit an increased intrinsic CH<sub>3</sub>OH formation rate normalized by the mass of copper compared to the Cu/SiO<sub>2</sub> reference catalyst, while the intrinsic CO

formation rate is rather similar for all samples (Figure 3a). The CH<sub>3</sub>OH selectivity, extrapolated to low conversion, is much higher for Cu/ZrO<sub>2</sub> and Cu/Zr<sub>0.9</sub>@SiO<sub>2</sub> (69 and 77 %, respectively) than for Cu/SiO<sub>2</sub> (48 %), Figure 3a. The Zr<sub>0.9</sub>@SiO<sub>2</sub> support itself shows no activity in CO<sub>2</sub> hydrogenation.

The evolution of the formation rates with respect to the contact time shows that CH<sub>3</sub>OH formation rate is indeed initially high for the zirconium-containing catalysts, but it drops down to a similar value as what is found for Cu/SiO<sub>2</sub> at longer contact time i.e. higher conversion (Figure 3b and Figure A.8-A.10). This likely indicates inhibition from the hydrogenation products (CH<sub>3</sub>OH or H<sub>2</sub>O) that block the Lewis acidic zirconium-sites. In contrast, the formation rate for CO is constant and similar for Cu/SiO<sub>2</sub> and Cu/Zr<sub>0.9</sub>@SiO<sub>2</sub> (Figure 3c) implying that the sites for CO formation is not easily inhibited and that CO is formed on different sites than CH<sub>3</sub>OH. Reducing the zirconium loading in Cu/Zr<sub>0.4</sub>@SiO<sub>2</sub> decreases the CH<sub>3</sub>OH formation rate, while the CO formation rate remains similar, further illustrating the importance of Zr surface density on CH<sub>3</sub>OH formation (Table A.2 and Figure A.11). In addition, the catalytic performance of monoclinic ZrO<sub>2</sub> has a similar selectivity pattern and activity per gram of Cu as the mainly tetragonal ZrO<sub>2</sub> support (Table A.2 and Figure A.12-A.15), showing that there are no significant qualitative differences between the crystalline phases. Lastly, after 48 hours of reaction, the activity and selectivity remain similar, demonstrating the stability of the catalyst. In fact, no significant sintering of the copper nanoparticle is observed (no significant changes in particle size and distribution - Figure A.16-A.18). Cu/ZrO<sub>2</sub> and Cu/Zr<sub>0.9</sub>@SiO<sub>2</sub> have very similar activity and selectivity patterns, with an increased formation rate for CH<sub>3</sub>OH compared to Cu/SiO<sub>2</sub>. This already points to the existence of similar active sites and mechanisms in both systems for the formation of CH<sub>3</sub>OH.



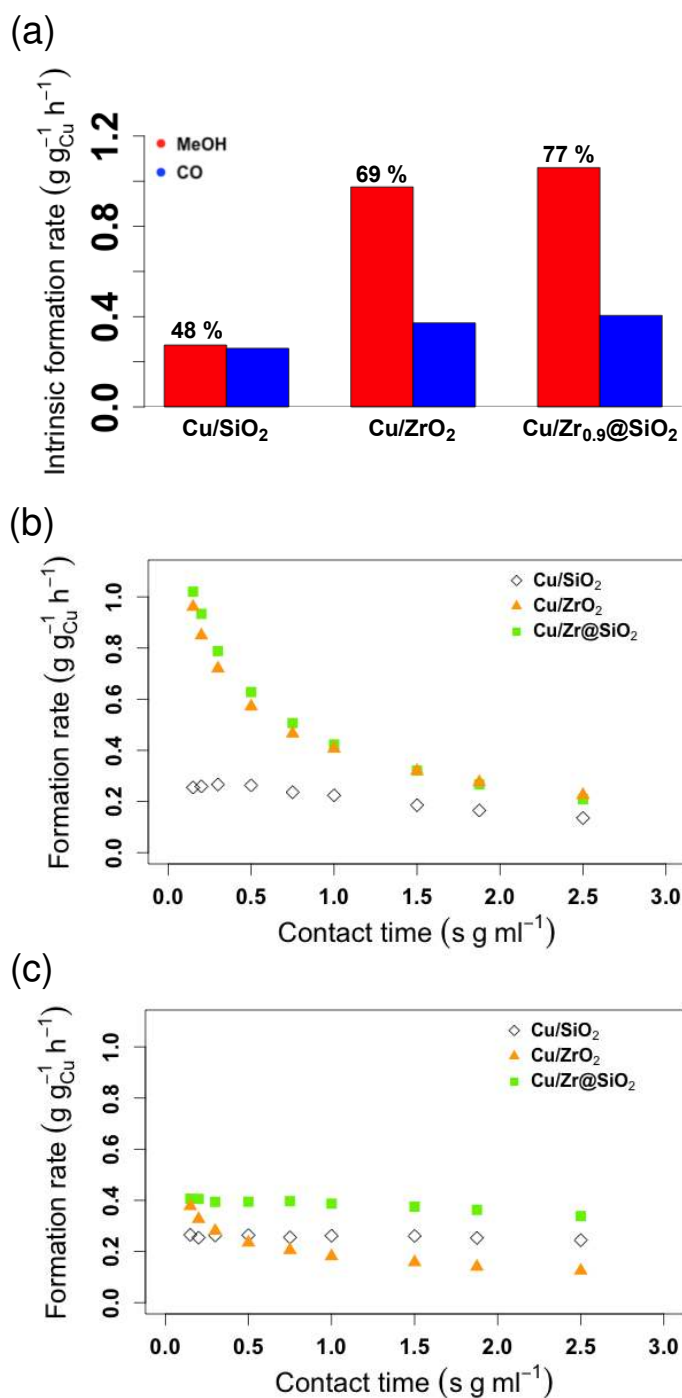


**Figure 3.** (a) Intrinsic formation rates of CH<sub>3</sub>OH (red) and CO (blue) for Cu/SiO<sub>2</sub>, Cu/ZrO<sub>2</sub>, and Cu/Zr<sub>0.9</sub>@SiO<sub>2</sub> by extrapolation to 0% conversion with the corresponding selectivity for CH<sub>3</sub>OH. Formation rates for CH<sub>3</sub>OH (b) and CO (c) with respect to the contact time for Cu/SiO<sub>2</sub>, Cu/ZrO<sub>2</sub>, and Cu/Zr<sub>0.9</sub>@SiO<sub>2</sub>. By comparison, the formation rate of CO on Cu/ZrO<sub>2</sub> decreases with contact time, implying that the formation of CO might also involve Lewis acidic Zr-sites.

### 2.3. In-situ XAS

To investigate the nature of both the Cu and the Zr-species under CO<sub>2</sub> hydrogenation conditions, in situ XAS experiments at the Cu and Zr K-edge are performed for Cu/Zr<sub>0.9</sub>@SiO<sub>2</sub>. First, spectra are recorded after exposure to air, then after heating at 300 °C under a flow of N<sub>2</sub>, during reduction with H<sub>2</sub> (300 °C and 1 bar) and finally under CO<sub>2</sub> hydrogenation conditions (CO<sub>2</sub>:H<sub>2</sub> in a 1:3 ratio, 230°C and 5 bars) (see temperature and gas flow scheme in Figure A.19). According to the Cu K-edge XANES spectra, copper is present as CuO upon exposure to air and reduces to Cu<sub>0</sub> under H<sub>2</sub> at 300 °C. No change of oxidation state of Cu is observed under CO<sub>2</sub> hydrogenation conditions at 230 °C and 5 bars (Figure A.20). The Zr K-edge spectra show no change in the position of the inflexion points (at 18002.0 and 18013.2 eV), indicating that the oxidation state of zirconium remains the same, i.e. Zr(IV), all along the in situ experiment. However, changes in the shape of the XANES spectra are observed. The XANES spectra after exposure to air show the absence of the pre-edge feature present in the ex situ sample recorded under inert atmosphere (Figure 5a, black line). This is consistent with a more centrosymmetric coordination environment around zirconium i.e. increase in coordination number, tentatively assigned to the adsorption of water from air moisture. The pre-edge feature reappears after heating under N<sub>2</sub>, very likely due to desorption of water regenerating Zr in a five-coordinated environment (Figure 4a - blue line, and the EXAFS spectrum in Figure A.21). Similar evolution is observed upon heating (300 °C) under a flow of compressed air, thus the change in EXAFS spectrum is solely related to the desorption of water and cannot be assigned to the formation of oxygen vacancies (Figure A.22). This data overall indicates that the changes observed upon exposure to air are reversible upon heating. No change of the zirconium K-edge spectra is observed during reduction with H<sub>2</sub>, neither in the XANES nor in EXAFS parts (Figure 4a, - green line and Figure A.21), confirming that neither reduction of Zr(IV) nor change in the zirconium-environment (e.g. formation of oxygen vacancies) takes place under these conditions. Under the reaction conditions (Figure 2.4a - red line), the pre-edge shows a slight decrease in intensity while the shape of the white line also changes.

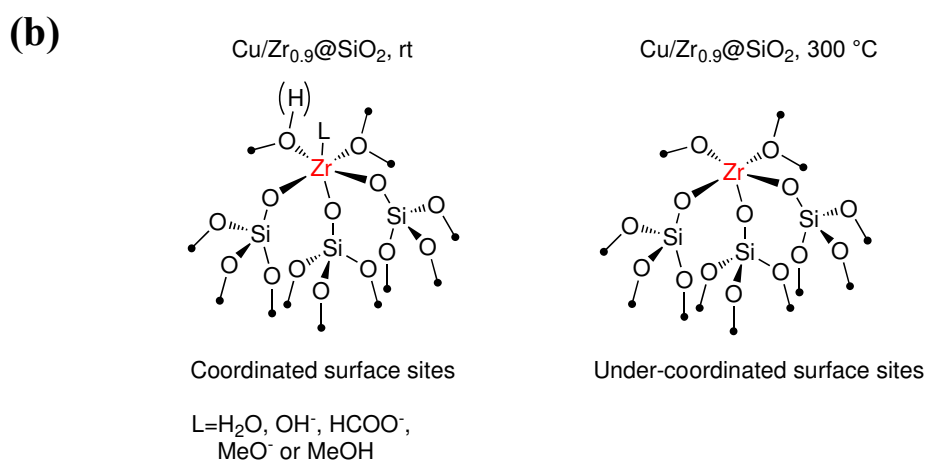
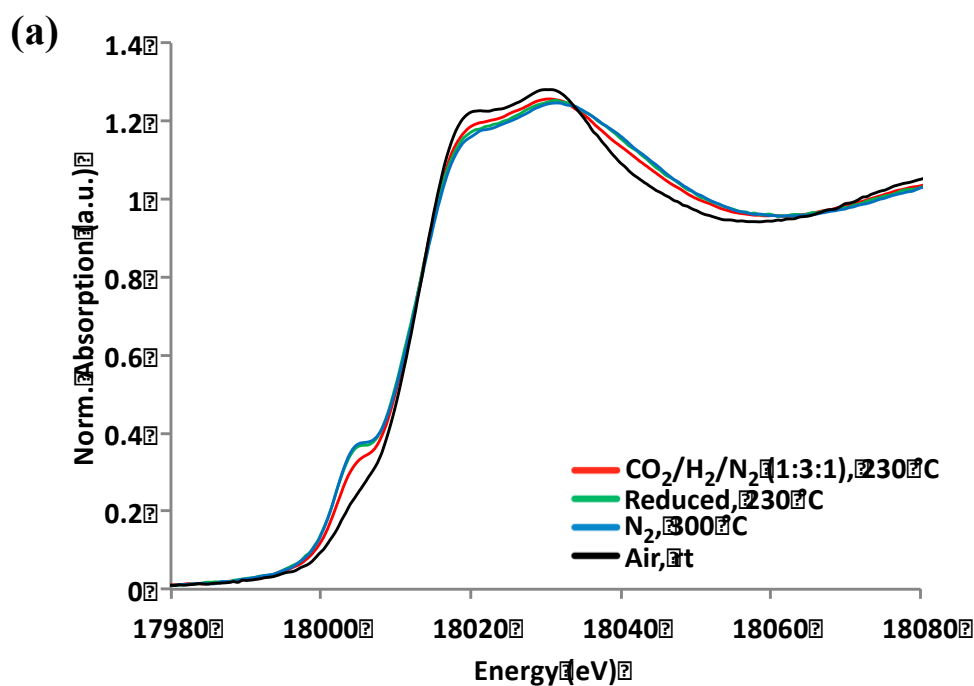


**Figure 4.** (a) Zirconium K-edge XANES spectra recorded at different stages under *in-situ* CO<sub>2</sub> hydrogenation of Cu/Zr<sub>0.9</sub>@SiO<sub>2</sub>. (b) Representation of the zirconium site used for XANES fitting with Cu/Zr<sub>0.9</sub>@SiO<sub>2</sub> at room temperature or at 300 °C to represent surface sites with and without substrates coordinated, respectively.

This change is unlikely associated to the change in oxidation state as the inflexion points remain at similar positions. In fact, the spectrum under reaction condition is a linear combination of the spectra before and after the thermal treatment, i.e. in a centro- and non-centrosymmetric environment, respectively (Figure 4b). This could be associated with adsorption of reaction intermediates/products during CO<sub>2</sub> hydrogenation (methoxy, methanol, water, formate, carbonates...)[24] that completes the coordination sphere of zirconium, gaining

back a centrosymmetric environment. Overall, about 33 % of the zirconium sites have an increased coordination number under steady-state reaction conditions for this specific sample (Figure A.23 and Table A.3).

#### 2.4. Solid State NMR

To further characterize the adsorbed species on the zirconium-sites observed during *in-situ* XAS measurements,  $^1\text{H}$ ,  $^{13}\text{C}$ -CPMAS and  $^1\text{H}$ - $^{13}\text{C}$  HETCOR spectra are recorded. The  $\text{Cu}/\text{Zr}_{0.9}@/\text{SiO}_2$  is exposed to 5 bars of  $^1\text{H}_2:^{13}\text{CO}_2$  (3:1) for 12 hours at 230 °C followed by evacuating the gas phase at room temperature. Analysis of the gas phase by solution NMR in  $\text{C}_6\text{D}_6$  confirmed the formation of  $\text{CH}_3\text{OH}$  from  $\text{CO}_2$  and  $\text{H}_2$  (Figure A.24-A.25), and the resulting solid-state  $^{13}\text{C}$  NMR spectrum shows two signals at 49 ppm and 170 ppm indicating two distinct carbon species (Figure A.26), assigned to methoxy and formate species coordinated to the support, respectively, as confirmed by  $^1\text{H}$ - $^{13}\text{C}$  HETCOR experiments (Figure 5).<sup>[58]</sup> Similar species have been previously observed on  $\text{Cu}/\text{ZrO}_2$ , while no signals are observed in the absence of copper or zirconium for  $\text{Zr}_{0.9}@/\text{SiO}_2$  or  $\text{Cu}/\text{SiO}_2$ , respectively, pointing out the synergy between the copper nanoparticles and the isolated Zr(IV) site.<sup>[24]</sup> Thus, the observed species are very likely adsorbed on the Zr(IV) sites dispersed at the surface of the support. Similar spectroscopic features regarding reaction intermediates and selectivity patterns are observed on  $\text{Cu}/\text{Zr}_{0.9}@/\text{SiO}_2$  and  $\text{Cu}/\text{ZrO}_2$ . This indicates that in both cases  $\text{CO}_2$  hydrogenation proceeds through similar mechanisms, reaction intermediates and active sites, involving the adsorption and conversion of  $\text{CO}_2$  and intermediates, likely at the perimeter between the copper particles and surface zirconium sites.

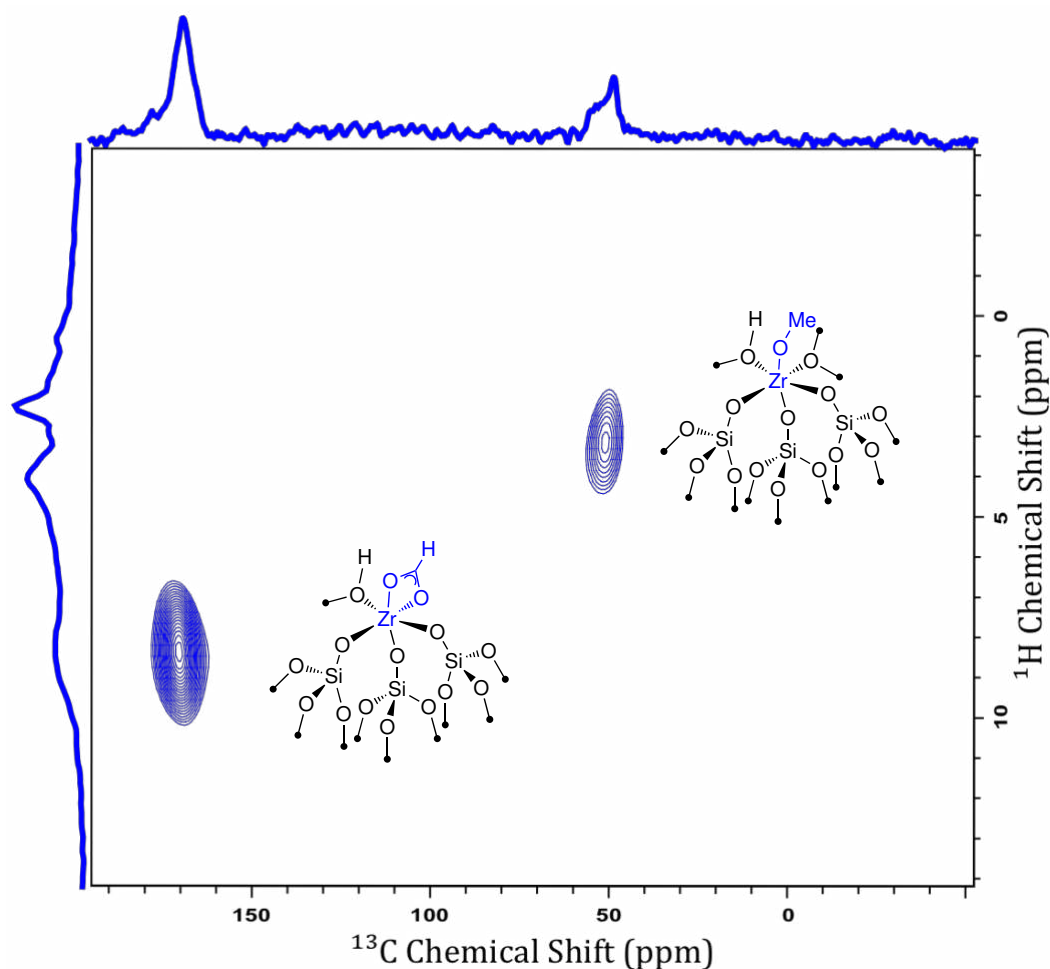


**Figure 5.** Ex situ  $^1\text{H}$ - $^{13}\text{C}$  HETCOR spectrum of  $\text{Cu}/\text{Zr}_{0.9}@/\text{SiO}_2$  after exposure to  $^{13}\text{CO}_2:1\text{H}_2$  in a 3:1 ratio at 5 bars and 230 °C.

## 2.3 Conclusion

Using a surface organometallic chemistry approach, we have prepared copper nanoparticles supported on silica containing isolated and well-dispersed Zr(IV) species ( $\text{Zr}_{0.9}@/\text{SiO}_2$ ). This catalyst showed improved performances in the hydrogenation of  $\text{CO}_2$  to  $\text{CH}_3\text{OH}$  compared to non Zr-promoted  $\text{Cu}/\text{SiO}_2$ , reaching similar selectivities as observed with  $\text{Cu}/\text{ZrO}_2$ . It shows that the structural and bulk properties of  $\text{ZrO}_2$  (oxygen vacancies...) are not required and that the presence of isolated Lewis acidic zirconium sites on the surface of silica, on which Cu nanoparticles are supported, is sufficient to trigger the increase of  $\text{CH}_3\text{OH}$  activity/selectivity. In fact, similar surface intermediates – formate and methoxy – are observed by solid-state NMR for  $\text{Cu}/\text{Zr}_{0.9}@/\text{SiO}_2$  and  $\text{Cu}/\text{ZrO}_2$ , while they are not observed on  $\text{Cu}/\text{SiO}_2$ . These observations speak for similar mechanisms of  $\text{CO}_2$  activation and active sites for the

formation of CH<sub>3</sub>OH. In situ XAS reveals that the isolated Zr(IV) sites do not change oxidation state in Zr<sub>0.9</sub>@SiO<sub>2</sub> under reaction conditions or pretreatment. Furthermore, the defect sites often invoked for Cu/ZrO<sub>2</sub> (like oxygen vacancies) cannot form on this system, thus they are likely not required to promote CO<sub>2</sub> hydrogenation. Thus, the role of surface Zr(IV) Lewis acid sites is likely to assist CO<sub>2</sub> activation and hydrogenation of reaction intermediates, consistent with our previous study. This study paves the way toward a rational design of CO<sub>2</sub> hydrogenation catalysts.

## 5 References

- [1] P. J. A. Tijm, F. J. Waller, D. M. Brown, *Appl. Catal. A: Gen.* **2001**, *221*, 275-282.
- [2] G. Olah, A. Goepfert, S. G. K. Prakash, *Beyond Oil and Gas: The Methanol Economy*, 2nd ed., Wiley-VCH: Weinheim, Germany, **2011**.
- [3] A. Álvarez, A. Bansode, A. Urakawa, A. V. Bavykina, T. A. Wezendonk, M. Makkee, J. Gascon, F. Kapteijn, *Chem. Rev.* **2017**, *117*, 9804-9838.
- [4] A. Goepfert, M. Czaun, J.-P. Jones, G. K. Surya Prakash, G. A. Olah, *Chem. Soc. Rev.* **2014**, *43*, 7995-8048.
- [5] A. Olah George, *Angew. Chem., Int. Ed.* **2012**, *52*, 104-107.
- [6] O. Martin, J. Martín Antonio, C. Mondelli, S. Mitchell, F. Segawa Takuya, R. Hauert, C. Drouilly, D. Curulla-Ferré, J. Pérez-Ramírez, *Angew. Chem., Int. Ed.* **2016**, *55*, 6261-6265.
- [7] H. Sakurai, S. Tsubota, M. Haruta, *Appl. Catal., A* **1993**, *102*, 125-136.
- [8] A. Baiker, M. Kilo, M. Maciejewski, S. Menzi, A. Wokaun, in *Stud. Surf. Sci. Catal.* **1993**, *75*, 1257-1272.
- [9] T. Fujitani, M. Saito, Y. Kanai, T. Watanabe, J. Nakamura, T. Uchijima, *Appl. Catal., A* **1995**, *125*, L199-L202.
- [10] F. Studt, I. Sharafutdinov, F. Abild-Pedersen, C. F. Elkjær, J. S. Hummelshøj, S. Dahl, I. Chorkendorff, J. K. Nørskov, *Nature Chem.* **2014**, *6*, 320.
- [11] J. Wang, G. Li, Z. Li, C. Tang, Z. Feng, H. An, H. Liu, T. Liu, C. Li, *Sci. Adv.* **2017**, *3*.
- [12] L. C. Grabow, M. Mavrikakis, *ACS Catal.* **2011**, *1*, 365-384.
- [13] E. M. Fiordaliso, I. Sharafutdinov, H. W. P. Carvalho, J.-D. Grunwaldt, T. W. Hansen, I. Chorkendorff, J. B. Wagner, C. D. Damsgaard, *ACS Catal.* **2015**, *5*, 5827-5836.
- [14] M. Behrens, R. Schlögl, *Z. Anorg. Allg. Chem.* **2013**, *639*, 2683-2695.

- [15] I. Kasatkin, P. Kurr, B. Kniep, A. Trunschke, R. Schlögl, *Angew. Chem. Int. Ed.* **2007**, *46*, 7324-7327.
- [16] M. Behrens, *J. Catal.* **2009**, *267*, 24-29.
- [17] S. Zander, L. Kunkes Edward, E. Schuster Manfred, J. Schumann, G. Weinberg, D. Teschner, N. Jacobsen, R. Schlögl, M. Behrens, *Angew. Chem. Int. Ed.* **2013**, *52*, 6536-6540.
- [18] A. Bansode, A. Urakawa, *J. Catal.* **2014**, *309*, 66-70.
- [19] R. Gaikwad, A. Bansode, A. Urakawa, *J. Catal.* **2016**, *343*, 127-132.
- [20] J. C. J. Bart, R. P. A. Sneeden, *Catal. Today* **1987**, *2*, 1-124.
- [21] G. C. Chinchin, P. J. Denny, D. G. Parker, M. S. Spencer, D. A. Whan, *Appl. Catal.* **1987**, *30*, 333-338.
- [22] I. A. Fisher, H. C. Woo, A. T. Bell, *Catal. Lett.* **1997**, *44*, 11-17.
- [23] I. A. Fisher, A. T. Bell, *J. Catal.* **1997**, *172*, 222-237.
- [24] K. Larmier, W. C. Liao, S. Tada, E. Lam, R. Verel, A. Bansode, A. Urakawa, A. Comas-Vives, C. Copéret, *Angew. Chem., Int. Ed.* **2017**, *56*, 2318-2323.
- [25] I. Ro, Y. Liu, M. R. Ball, D. H. K. Jackson, J. P. Chada, C. Sener, T. F. Kuech, R. J. Madon, G. W. Huber, J. A. Dumesic, *ACS Catal.* **2016**, *6*, 7040-7050.
- [26] T. Witoon, J. Chalorntham, P. Dumrongbunditkul, M. Chareonpanich, J. Limtrakul, *Chem. Eng. J.* **2016**, *293*, 327-336.
- [27] K. T. Jung, A. T. Bell, *Catal. Lett.* **2002**, *80*, 63-68.
- [28] S. Tada, A. Katagiri, K. Kiyota, T. Honma, H. Kamei, A. Nariyuki, S. Uchida, S. Satokawa, *J. Phys. Chem. C* **2018**, *122*, 5430-5442.
- [29] S. Tada, K. Larmier, R. Buchel, C. Coperet, *Catal. Sci. Technol.* **2018**, *8*, 2056-2060.
- [30] S. Tada, F. Watanabe, K. Kiyota, N. Shimoda, R. Hayashi, M. Takahashi, A. Nariyuki, A. Igarashi, S. Satokawa, *J. Catal.* **2017**, *351*, 107-118.
- [31] F. Arena, G. Italiano, K. Barbera, S. Bordiga, G. Bonura, L. Spadaro, F. Frusteri, *Appl. Catal., A* **2008**, *350*, 16-23.
- [32] T. C. Schilke, I. A. Fisher, A. T. Bell, *Catal. Lett.* **1998**, *54*, 105-111.
- [33] T. C. Schilke, I. A. Fisher, A. T. Bell, *J. Catal.* **1999**, *184*, 144-156.
- [34] C. Schild, A. Wokaun, A. Baiker, *J. Mol. Catal.* **1990**, *63*, 243-254.
- [35] J. Weigel, R. A. Koepfel, A. Baiker, A. Wokaun, *Langmuir* **1996**, *12*, 5319-5329.
- [36] A. Wokaun, J. Weigel, M. Kilo, A. Baiker, *Fresenius. J. Anal. Chem.* **1994**, *349*, 71-75.

- [37] M. Behrens, F. Studt, I. Kasatkin, S. Kühn, M. Hävecker, F. Abild-Pedersen, S. Zander, F. Girgsdies, P. Kurr, B.-L. Kniep, M. Tovar, R. W. Fischer, J. K. Nørskov, R. Schlögl, *Science* **2012**, *336*, 893.
- [38] J. D. Grunwaldt, A. M. Molenbroek, N. Y. Topsøe, H. Topsøe, B. S. Clausen, *J. Catal.* **2000**, *194*, 452-460.
- [39] T. Fujitani, J. Nakamura, *Cat. Lett.* **1998**, *56*, 119-124.
- [40] T. Fujitani, I. Nakamura, T. Uchijima, J. Nakamura, *Surf. Sci.* **1997**, *383*, 285-298.
- [41] E. L. Kunkes, F. Studt, F. Abild-Pedersen, R. Schlögl, M. Behrens, *J. Catal.* **2015**, *328*, 43-48.
- [42] S. Kuld, M. Thorhauge, H. Falsig, C. F. Elkjær, S. Helveg, I. Chorkendorff, J. Sehested, *Science* **2016**, *352*, 969.
- [43] T. Lunkenbein, J. Schumann, M. Behrens, R. Schlögl, G. Willinger Marc, *Angew. Chem. Int. Ed.* **2015**, *54*, 4544-4548.
- [44] S. Kattel, B. Yan, Y. Yang, J. G. Chen, P. Liu, *J. Am. Chem. Soc.* **2016**, *138*, 12440-12450.
- [45] Y. H. Wang, W. G. Gao, H. Wang, Y. E. Zheng, W. Na, K. Z. Li, *RSC Adv.* **2017**, *7*, 8709-8717.
- [46] K. Samson, M. Śliwa, R. P. Socha, K. Góra-Marek, D. Mucha, D. Rutkowska-Zbik, J. F. Paul, M. Ruggiero-Mikołajczyk, R. Grabowski, J. Słoczyński, *ACS Catal.* **2014**, *4*, 3730-3741.
- [47] J. C. Frost, *Nature* **1988**, *334*, 577.
- [48] C. Copéret, D. P. Estes, K. Larmier, K. Searles, *Chem. Rev.* **2016**, *116*, 8463-8505.
- [49] C. Copéret, A. Comas-Vives, M. P. Conley, D. P. Estes, A. Fedorov, V. Mougel, H. Nagaie, F. Núñez-Zarur, P. A. Zhizhko, *Chem. Rev.* **2016**, *116*, 323-421.
- [50] C. Copéret, M. Chabanas, R. Petroff Saint-Arroman, J. M. Basset, *Angew. Chem. Int. Ed.* **2003**, *42*, 129-129.
- [51] E. Lam, K. Larmier, P. Wolf, S. Tada, O. V. Safonova, C. Copéret, *J. Am. Chem. Soc.* **2018**, *140*, 10530-10535.
- [52] H. Davis Burtron, *J. Am. Ceram. Soc.* **2006**, *67*, C-168-C-168.
- [53] K. W. Terry, C. G. Lugmair, T. D. Tilley, *J. Am. Chem. Soc.* **1997**, *119*, 9745-9756.
- [54] A. Roussey, P. Gentile, D. Lafond, E. Martinez, V. Jousseume, C. Thieuleux, C. Coperet, *J. Mater. Chem. C* **2013**, *1*, 1583-1587.



- [55] B. O. Wagner, G. S. Hammond, *J. Organomet. Chem.* **1975**, *85*, 1-14.
- [56] K. Larmier, S. Tada, A. Comas-Vives, C. Copéret, *J. Phys. Chem. Lett.* **2016**, *7*, 3259-3263.
- [57] O. Muller, M. Nachtegaal, J. Just, D. Lutzenkirchen-Hecht, R. Frahm, *J. Synchrotron Radiat.* **2016**, *23*, 260-266.
- [58] F. Rataboul, A. Baudouin, C. Thieuleux, L. Veyre, C. Copéret, J. Thivolle-Cazat, J.-M. Basset, A. Lesage, L. Emsley, *J. Am. Chem. Soc.* **2004**, *126*, 12541-12550.
- [59] F. Meneghetti, E. Wendel, S. Mascotto, B. M. Smarsly, E. Tondello, H. Bertagnolli, S. Gross, *CrystEngComm* **2010**, *12*, 1639-1649.
- [60] G. Mountjoy, D. M. Pickup, R. Anderson, G. W. Wallidge, M. A. Holland, R. J. Newport, M. E. Smith, *Phys. Chem. Chem. Phys.* **2000**, *2*, 2455-2460.
- [61] S. Foraita, L. Fulton John, A. Chase Zizwe, A. Vjunov, P. Xu, E. Baráth, M. Camaioni Donald, C. Zhao, A. Lercher Johannes, *Chem. Eur. J.* **2014**, *21*, 2423-2434.
- [62] M. Steib, Y. Lou, A. Jentys, A. Lercher Johannes, *ChemCatChem* **2017**, *9*, 3809-3813.
- [63] W. R. Gunther, V. K. Michaelis, R. G. Griffin, Y. Román-Leshkov, *J. Phys. Chem. C* **2016**, *120*, 28533-28544.